Electronic Supplementary Information (ESI)

Hierarchical bicontinuous structure of redox-active organic composites and their enhanced electrochemical properties

Kosuke Sato, Mirei Arayasu, Hirotaka Masaki, Hiroaki Imai, Yuya Oaki*

Department of Applied Chemistry, Faculty of Science and Technology, Keio University, 3-14-1 Hiyoshi, Kohoku-ku, Yokohama 223-8522, Japan.

E-mail: oakiyuya@applc.keio.ac.jp

Contents

Experimental methods

Synthesis of the quinone/PPy composite. All the reagents were used as purchased without purification. Three quinone derivatives, such as 2-chloro-5-methyl-1,4-benzoquinone (CMBQ, TCI, 98.0%), 2,5-dichloro-1,4-benzoquinone (DCBQ, TCI, 98.0%) and tetrachloro-1,4-benzoquinone (TCBQ, TCI, 98.0%), were set in a polypropylene vessel 120 cm^3 in volume. These quinone crystals were packed into the pellet 13 mm in diameter. A small glass bottle containing 1 cm^3 of pyrrole (Py, TCI, 99.0%) monomer liquid was separately put in the vessel. The sealed outer vessel was maintained at 60 °C for certain period, typically 24 h. The excess monomer was evaporated at 60 °C with opening of the seal. When the quinone derivatives were removed, the composite samples were immersed in acetone for 24 h.

Structure characterization. The morphologies were observed by optical microscopy (Keyence, VHX-1000) and field-emission scanning electron microscopy (SEM, Hitachi S-4700, and JEOL JSM7600F) operated at 3.0 kV. The composition of the resultant composites was characterized by Fourier-transform infrared (FT-IR) absorption spectroscopy (FT-IR, JASCO, FT/IR-4200). The samples for FT-IR analysis were prepared by mixing with potassium bromide (KBr). The structure changes of the quinone crystals were analyzed by X-ray diffraction (XRD, Rigaku Mini Flex II) with Cu-Kα radiation. The content of PPy in the composites was estimated from thermogravimetric analysis (TG, Seiko TG/DTA7200) under air condition.

Electrochemical properties. The electrochemical measurement was performed by using a three electrode setup in a twin-beaker cell. The resultant QN/PPy composites were used as the active material. The working electrode was prepared by mixing of 80 wt-% active materials, 10 wt-% acetylene black carbon, and 10 wt-% poly(vinylidene fluoride) (PVDF). The slurry of these materials with small amount of *N*-methyl-2-pyrrolidone (Junsei Chemical, 99%) was dropped on a titanium mesh as a current collector. A platinum wire and Ag/AgCl electrode were used as the counter and reference electrodes, respectively. The electrolyte was 1 mol dm^{-3} sulfuric acid (H_2SO_4) aqueous solution. Chronopotentiometry was performed by using charge-discharge measurement system (Hokuto Denko, HJ1001SD8) in the same potential range at the different current density.

Composition and morphology of PPy/TCBQ composites

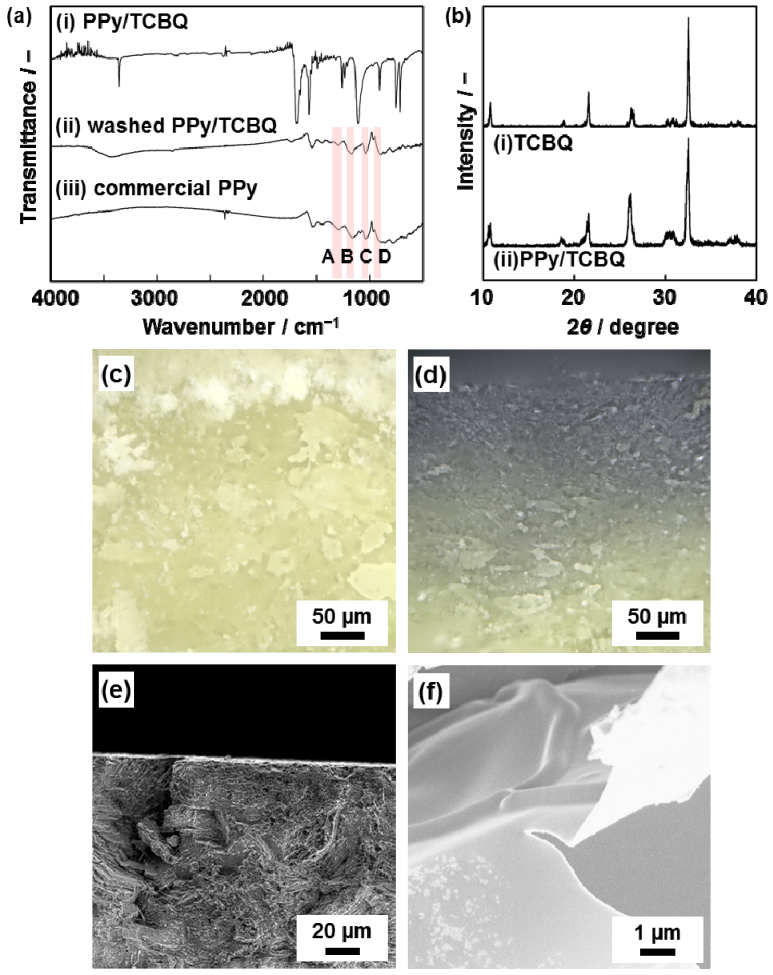

Fig. S1. Composition and morphology of the PPy/TCBQ. (a) FT-IR spectra of the PPy/TCBQ composite before (i) and after (ii) removal of TCBQ by immersion in acetone and commercial PPy (iii). The absorption bands with red band (A–D) were characteristic to those of PPy, as described in the note of the main text. (b) XRD patterns of TCBQ bulk crystal (i) and the resultant PPy/TCBQ composite (ii). (c,d) Cross-sectional optical microscopy images of the original TCBQ pellet (c) and that after the polymerization with Py (d). (e,f) SEM images of the TCBQ/PPy before (e) and after (f) dissolution of TCBQ by acetone.

The absorption bands characteristic to PPy were not observed on the FT-IR spectrum of the PPy/TCBQ. The absorption bands assigned to PPy appeared after dissolution of TCBQ by acetone (Fig. S1a). The XRD pattern of the PPy/TCBQ showed the peaks corresponding to TCBQ (Fig. S1b). The TCBQ pellet consisted of the crystals 5–50 μm in size (Fig. S1c). After the polymerization, the color change was observed near the surface layer (Fig. S1d). The PPy content was estimated to be 0.1 wt% from the TG analysis (Fig. S2). These results suggest that formation of PPy proceeds only on the surface layer of the TCBQ pellet (Fig. S1e). Therefore, the PPy nanosheets were obtained after dissolution of TCBQ (Fig. S1f). The sufficient amount of PPy was not formed in the PPy/TCBQ. Since the lower solubility of TCBQ to Py directs the slower etching and polymerization rate, the formation of PPy only proceeds on the surface of the pellet.

In Fig. 2a and Fig. S1a, the absorption bands A−D are assigned to PPy as follows:[15] C=C stretching vibration and C=C–C ring in-plane deformation (A), C–C in-ring stretching vibration (B), C–H ring out-of-plane bending vibration (C), and C=C stretching vibration and C=C–C ring out-plane deformation (D).[15] The absorption bands E–I are assigned to quinone derivatives and their reduced compounds as follows: O–H stretching vibration (E), C=O stretching vibration (F), aromatic C=C stretching vibration (G), aromatic C–H out-plane deformation (H), C–H out-plane deformation (I).

TG curves of the composites

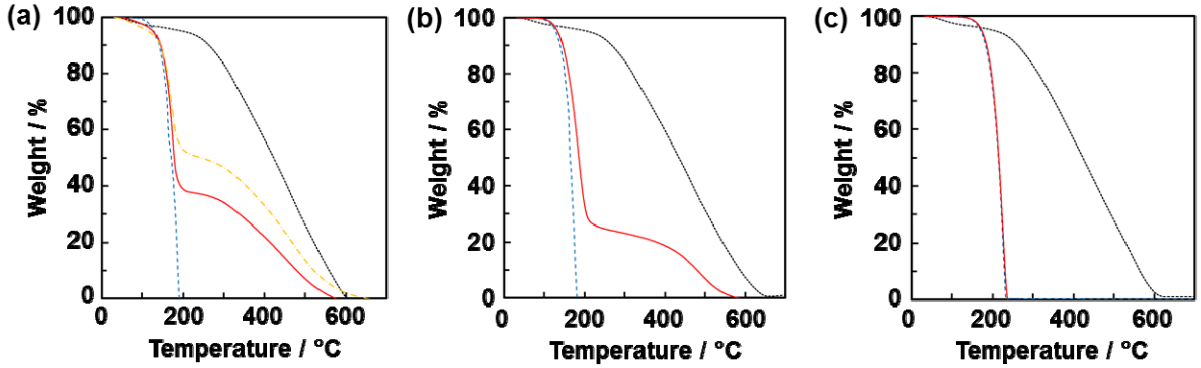

Fig. S2. TG curves of the PPy/CMBQ (a), PPy/DCBQ (b), and PPy/TCBQ (c) related samples and their related samples. (a) PPy/CMBQ composite (red line), commercial CMBQ crystal (blue dashed line), commercial PPy (black dotted line), and PPy/CMBQ composite after removal of the micrometer-sized CMBQ crystals under vacuum drying (yellow dashed line). (b) PPy/DCBQ composite (red line), commercial DCBQ crystal (blue dashed line), and commercial PPy (black dotted line). (c) PPy/TCBQ (red line), commercial TCBQ crystal (blue broken line), and commercial PPy (black dotted line).

The TG curves of the composites consisted of two-step weight loss around 200 °C and 250–400 °C respectively corresponding to combustion of the quinone derivatives and PPy. Based on the weight loss, the PPy contents were estimated to be 40 wt% for PPy/CMBQ, 24 wt% for PPy/DCBQ, and 0.12 wt% for PPy/TCBQ. The PPy content of the PPy/CMBQ was increased from 40 wt% to 56 wt% after the sublimation of CMBQ embedded in the microscale bicontinuous morphology by vacuum drying.

Composition and morphology of the PPy/CMBQ with different reaction time

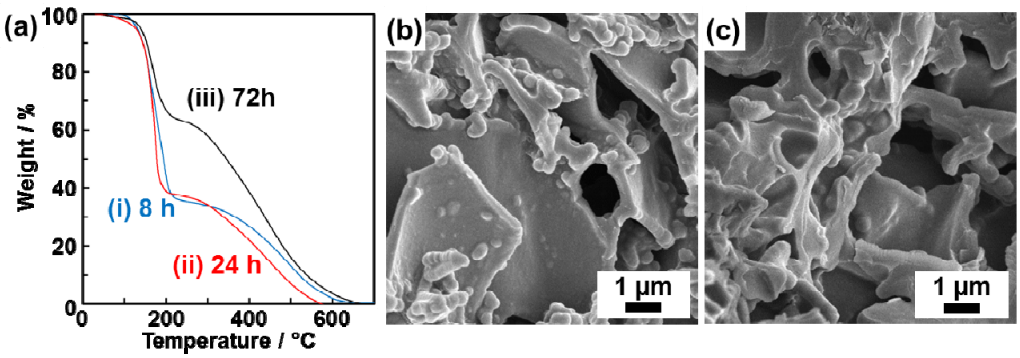

Fig. S3. TG curves (a) and SEM images (b,c) of the PPy/CMBQ composites with the different reaction time. (a) PPy/CMBQ composites at the reaction time for 8 h (i, blue line), 24 h (ii, red line), and 72h (iii, black line), (b, c) SEM images of the PPy/CMBQ composite at the reaction time for 8 h (b) and 24 h (c).

Based on the TG curves, the CMBQ content in PPy/CMBQ was estimated to be 65 wt%, 60 wt%, 37 wt% at the reaction time for 8 h, 24 h, and 72 h, respectively (Fig. S3a). The generation of PPy and the sublimation of CMBQ cause the decrease in the CMBQ composition. The slight morphology changes of the composite were observed by the polymerization of Py and the etching and sublimation of CMBQ (Fig. 3e and Fig. S3b,c). The specific capacity of the PPy/CMBQ composites at the reaction time for 8 h, 24 h, and 72 h was 94 mA h g^{-1}, 110 mA h g^{-1}, and 39 mA h g^{-1} at the current density of 0.5 A g^{-1}.

Electrochemical properties of the PPy sample obtained from the PPy/CMBQ composite

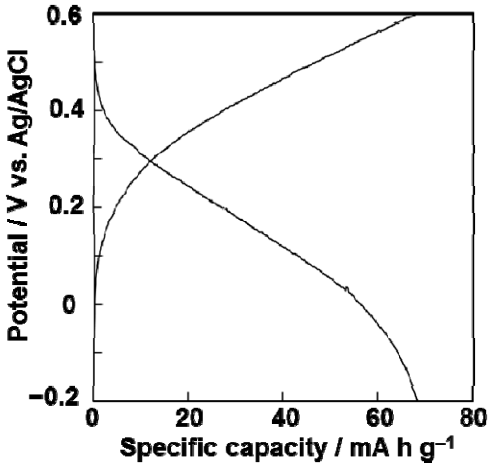

Fig. S4. Charge-discharge curve of the PPy sample after the dissolution of CMBQ from the PPy/CMBQ composite. The current density was 0.5 A g^{-1}.

The CMBQ was removed from the PPy/CMBQ composite (Fig. 3f). The resultant PPy showed the linear change of the potential in 0–0.6 V based on the redox reaction with the doping and dedoping.[9]

Reproducibility of the electrochemical properties

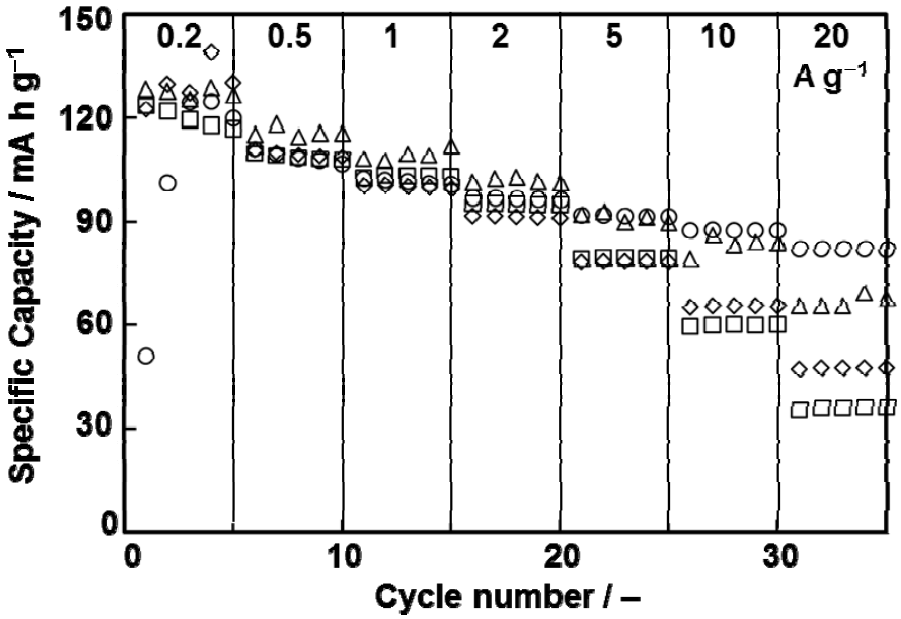

Fig. S5. Relationship between the current density and the specific capacity of the four PPy/CMBQ samples prepared in the same procedure.

The measured capacities are reproducible. The working electrode was prepared by mixing of the active material, the conductive carbon, and the binder in a mortar. The slight differences of the mixed and coating states caused the data variation especially in the high current density.

Cycle stability and coulombic efficiency of the PPy/CMBQ composites

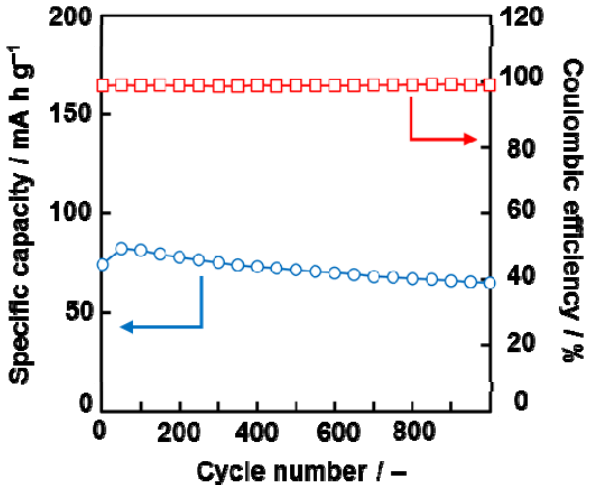

Fig. S6. Cycle stability (blue circles in the left axis) and coulombic efficiency (red squares in the right axis) of the PPy/CMBQ hierarchical bicontinuous composite at 5 A g^{-1}.

The capacity retention of the PPy/CMBQ was 89% after 1000 cycle. The slight increase in the specific capacity in the initial cycles is ascribed to the penetration of the electrolyte solution into the hierarchical structures. The coulombic efficiency was kept at 99 % within the 1000 cycles.

Electrochemical properties of quinone-based composites in previous works

Table S1 Electrochemical properties of quinone derivatives loaded on nanocarbon matrices.

No.	Symbol	Specific capacity / mA h g^{-1}	Current density / A g^{-1}	Active material	Electrolyte	Ref
*	●	88	10	PPy/CMBQ	1 M H_2SO_4 aq	Present work
1	□	90	10	AQ adsorbed on activated carbon with the hierarchical tube structure	1 M H_2SO_4 aq	7*b*
2	◊	100	10	Hydroquinone (HQ) adsorbed on graphene oxide	1 M H_2SO_4 aq	7*d*
3	×	25	5.6	Anthraquinone (AQ) adsorbed on activated carbon	0.5 M H_2SO_4 aq	7*e*
4	♦	43	10	2-Aminoanthraquinone grafted on graphene oxide	1 M H_2SO_4 aq	7*f*
5	△	94	10	AQ adsorbed on graphene framework	1 M H_2SO_4 aq	7*g*
6	+	31	10	AQ adsorbed on activated carbon	1 M H_2SO_4 aq	7*h*
7	▲	66	10	Bisphenol A adsorbed on graphene hydrogel	1 M H_2SO_4 aq	7*i*
8	■	41	8	2-tert-butyl-hydroquinone adsorbed on graphene	1 M H_2SO_4 aq	7*j*
9	*	53	10	lignin nanocrystals confined on reduced graphene oxides	0.1 M $HClO_4$	7*l*

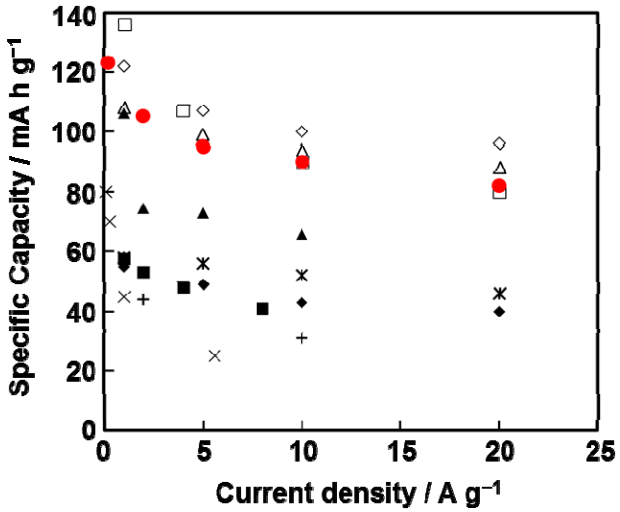

Fig. S7 Relationship between current density and specific capacity reported in previous works summarized in Table S1.

Table S1 and Fig. S7 summarizes the electrochemical properties of the quinone molecules adsorbed and/or loaded on nanocarbons in previous works. Our present work shows one of the highest enhanced electrochemical properties in view of the data variation.